J Comput Aided Mol Des (2009) 23:737–745
DOI 10.1007/s10822-009-9298-8

Studies of chirality effect of 4-(phenylamino)-pyrrolo[2,1-f][1,2,4]triazine on p38α by molecular dynamics simulations and free energy calculations

Quan Chen · Wei Cui · Mingjuan Ji

Received: 16 December 2008 / Accepted: 28 July 2009 / Published online: 12 August 2009

Abstract 4-(Phenylamino)-pyrrolo[2,1-f][1,2,4]triazines have been discovered as inhibitors of p38α. Experimental assays have proven that the configuration of α-Me-benzyl connected with amide at C6 is essential for the binding affinity. The S-configured inhibitor (11j) displays 80 times more potency than the R-configured one (11k). Here we investigated the mechanism how different configurations influence the binding affinity using molecular dynamics simulations, free energy calculations and free energy decomposition analysis. We found that the van der Waals interactions play the most important role in differentiating the activities between 11j and 11k with p38α. The difference of the van der Waals interactions is primarily determined by two residues, LEU108 and LEU167. Consequently stabilization of pyrrolo[2,1-f][1,2,4]triazine ring is important for the activities of inhibitors. Meanwhile we observed that the different configuration of the α-Me-benzyl group leads to the difference of binding between 11j and 11k. In conclusion, our work shows that it is feasible to analyze the chirality effect of inhibitors with different configurations by molecular dynamics simulations and free energy calculations, and provides useful information for drug design.

Keywords p38α · Molecular dynamics simulation · Binding free energy · Chirality · Inhibitor

Q. Chen · W. Cui · M. Ji (✉)
College of Chemistry and Chemical Engineering, Graduate University of Chinese Academy of Sciences, 100049 Beijing, People's Republic of China
e-mail: jmj@gucas.ac.cn; kejianjmj@gmail.com

Introduction

p38 is a family of serine/threonine mitogen-activated protein kinases, which plays an important role in inflammation. Activation of p38 leads to the up-regulation of TNFα and IL-1β [1–5], both of which are implicated in chronic inflammatory diseases [6]. Four isoforms of p38 have been identified, including p38α [7, 8], p38β [9], p38γ [10–12] and p38δ [13, 14]. Based on the size of the buried lipophilic pocket at the ATP site, p38α and p38β kinases form one subgroup, while p38γ and p38δ kinases segregate as another subgroup. It is believed that the predominant isoform involved in inflammation is p38α [15–17]. So p38α has emerged as an attractive target for the treatment of inflammatory diseases [1, 5, 18–22]. Designing of inhibitors to compete the binding of ATP is an important way for the discovery of new drugs. ATP binding site is a hydrophobic pocket of p38α formed by residues VAL38, ALA51, HIS107, LEU108, MET109, and LEU167 [23]. In addition, hydrogen bond interactions of inhibitors with GLU71, MET109, ASP168 are extensively adopted in drug design [23–26].

4-(Phenylamino)-pyrrolo[2,1-f][1,2,4]triazines substituted C6 with amide have been discovered as ATP competitive inhibitors of p38α [26]. Experimental assays indicate that the configuration of α-Me-benzyl connected with amide is crucial for the binding affinity, the S-configured inhibitor (11j) displayed 80 times more potency than the corresponding R-configured one (11k) [26]. In the current work, the binding mechanisms of the two inhibitors (see Fig. 1) were studied by molecular dynamics (MD) simulations, Molecular Mechanics/Poisson-Boltzmann Surface Area (MM/PBSA) free energy calculations [27–35], and Molecular Mechanics/Generalized Born Surface Area (MM/GBSA) free energy decomposition analysis [36–39]. We

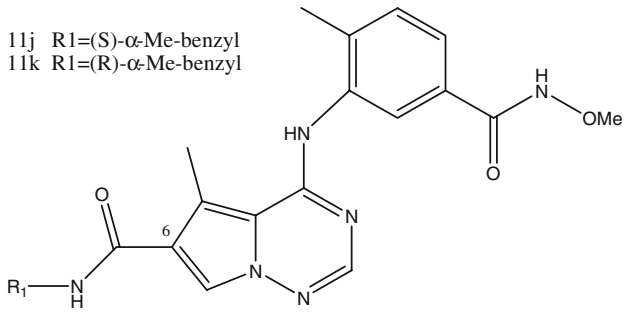

Fig. 1 Structures of 11j and 11k

expect that this work would provide a molecular basis for understanding how different configurations influence the binding affinity, and thus advance the rational design of this style of inhibitors.

Materials and methods

Starting structures

The X-ray structure of the 11j analogue in complex with p38α has been reported (PDB entry: 2RG5) [26], and the initial structures of 11j and 11k complexed with p38α were obtained by modifying the ligand in 2RG5. All above work was done in SYBYL7.1 [40]. The missing atoms of p38α were added using the *leap* program in AMBER9.0 [41]. AMBER03 force field was used for proteins [42].

The partial charges of the inhibitors were obtained as follows: first, the inhibitors with the Gasteiger–Huckel charges were minimized to a gradient of 0.001 kcal/(mol Å) in SYBYL7.1; then, further geometric optimization was performed at the Hartree-Fock level with the 6-31G* basis set using Gaussian03 [43]. Atomic charges of the inhibitors were obtained by fitting the electrostatic potentials calculated by Gaussian using the RESP technique [44]. Partial atomic charges and *gaff* force-field parameters for the inhibitors were generated by the *antechamber* program in AMBER9.0 [45].

Each complex was immersed in a truncated octahedron box of TIP3P waters [46]. Na^+ ions were added to neutralize the system using *leap* in AMBER9.0. The water box was extended 12 Å away from any solute atoms.

Molecular dynamics simulations

Prior to MD simulations, energy optimization was conducted using the *sander* program in AMBER9.0 by three steps. First, energy optimization was applied for water molecules (2,000 steps of the steepest descent and 2,000 steps of the conjugate gradient minimizations). Then, all backbone atoms were fixed, and the side-chains, inhibitor and solvent were optimized (5,000 steps of steepest descent and 10,000 steps of conjugate gradient minimizations). Finally, the whole system was optimized (5,000 steps of steepest descent and 5,000 steps of conjugate gradient minimizations) without any constrain.

During the first 60 ps of MD simulations, the temperature was increased from 0 to 310 K using the NVT ensemble. Initial velocities were assigned from a Maxwellian distribution at the starting temperature. Then, 4 ns MD simulations were performed under a constant temperature of 310 K using the weak-coupling algorithm [47]. During the MD simulations, SHAKE was used to fix all bonds involving hydrogen atoms and the time step was set to 2 fs [48]. Particle Mesh Ewald (PME) was employed for the long range electrostatic interactions [49]. During the sampling process coordinates were saved every 0.2 ps.

MM/PBSA calculations

MM/PBSA procedure was performed to calculate the absolute binding free energy of the inhibitors according to the following equation [34, 35]:

$$\begin{aligned}\Delta G_{\text{bind}} &= G_{\text{complex}} - G_{\text{protein}} - G_{\text{ligand}} \\ &= \Delta E_{\text{MM}} + \Delta G_{\text{PB}} + \Delta G_{\text{SA}} - T\Delta S\end{aligned} \quad (1)$$

where ΔE_{MM} is the molecular mechanics interaction energy between protein and inhibitor; ΔG_{PB} and ΔG_{SA} are the polar and non-polar free energy of solvation, respectively; $T\Delta S$ is the inhibitor entropic contribution at temperature T.

Here, the polar solvation energy was calculated by solving the Poisson–Boltzmann (PB) equations. The non-polar term was determined based on solvent-accessible surface area (SASA) determined by the LCPO method: $G_{\text{SA}} = 0.0072 \times \text{SASA}$ [50]. The protein-inhibitor binding free energy was calculated by averaging the 300 snapshots extracted from the MD trajectory from 1.0 to 4.0 ns. The conformational entropy was not considered here because of its high computational demand and relatively low accuracy of predictions.

Inhibitor–residue interaction decomposition

The interaction between inhibitor and each residue was computed using the MM/GBSA decomposition process by the *mm_pbsa* program in AMBER9.0 [38]. The binding interaction of each inhibitor–residue pair includes three energy terms: van der Waals contribution (ΔE_{vdw}), electrostatic contribution (ΔE_{ele}), and solvation contribution ($\Delta G_{\text{solvation}}$). The solvation free energy $\Delta G_{\text{solvation}}$ is

computed as the sum of the polar (ΔG_{GB}) and the non-polar (ΔG_{SA}) parts. The ΔG_{GB} term was computed using the generalized Born(GB) model and the parameters for GB were developed by Onufriev et al. [51]. The non-polar contribution (ΔG_{SA}) was determined based on solvent-accessible surface area determined with the ICOSA method. All energy components were calculated using the 300 snapshots extracted from the MD trajectory from 1.0 to 4.0 ns.

Results and discussion

The 4 ns MD trajectories of complexes consisting of inhibitors and p38α were generated. The atomic root-mean-square displacements (RMSD) of the protein structures are shown in Fig. 2. The RMSD plot indicates that the simulation of the p38α/11j complexe achieved equilibrium after 1 ns and were fluctuating around 2.06 Å. However, the RMSD fluctuation of p38α/11k is larger than that of p38α/11j which is fluctuating periodically on the whole. Moreover, we analyzed the fluctuations of the electrostatic and the van der Waals interactions between 11k and p38α (Figs. 3, 4), respectively. We found that both of them achieved equilibrium after 1 ns. Therefore, the free energy calculations based on the snapshots after 1.0 ns should be reliable.

More detailed analysis of root-mean-square fluctuation (RMSF) versus the residue number for the p38α/inhibitor complexes is illustrated in Fig. 5. From the plots, we observe that two of the complexes share similar RMSF. So they should have similar interaction mechanism with p38α on the whole.

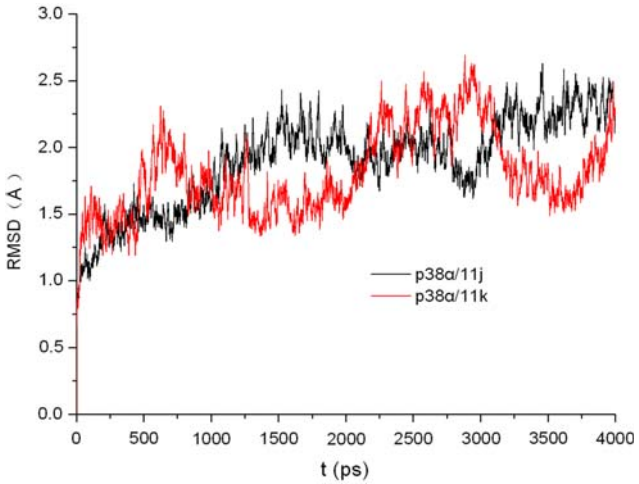

Fig. 2 RMSD of the backbone atoms of the p38α complexed with inhibitors

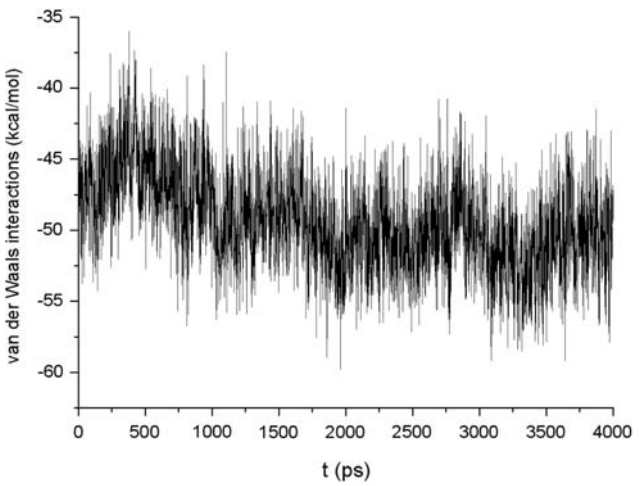

Fig. 3 Fluctuation of the van der waals interaction of the p38α/11k complex

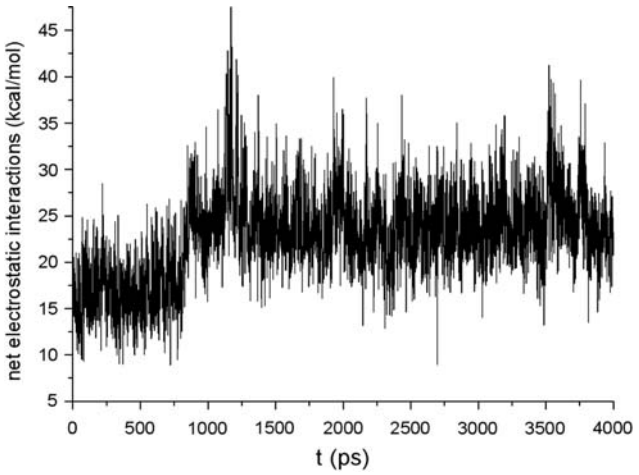

Fig. 4 Fluctuation of the electrostatic interaction of the p38α/11k complex

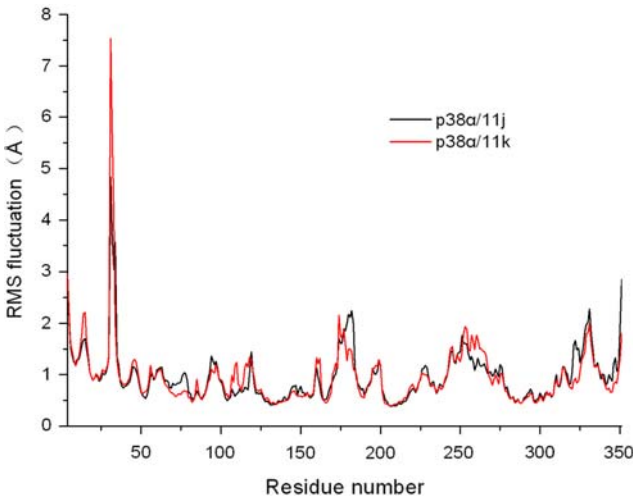

Fig. 5 RMSF of the backbone atoms of the p38α complexed with inhibitors

Table 1 Binding free energies and individual energy terms of 11j and 11k in complex with p38α (kcal/mol)

Inhibitor	ΔE_{vdw}	ΔE_{ele}	ΔG_{PB}	$\Delta E_{ele} + \Delta G_{PB}$	ΔG_{SA}	ΔG_{pred}	IC50 (nM)
11j	−57.35 ± 2.78	−28.31 ± 3.64	50.56 ± 4.07	22.25	−7.55 ± 0.15	−42.64 ± 3.94	2.2
11k	−48.82 ± 4.46	−21.78 ± 4.03	45.94 ± 4.90	24.16	−7.34 ± 0.33	−32.00 ± 5.01	180

Binding free energy

The absolute binding free energies of 11j and 11k using the MM/PBSA technique are shown in Table 1. The predicted binding free energies (ΔG_{pred}) of 11j and 11k are −42.64 and −32.00 kcal/mol, respectively. The predictions are in good agreement with the experimental results.

According to the energy components, ΔG_{PB} offsets the favorable electrostatic interaction, and the ΔG_{SA} term, which corresponds to the burial of SASA upon binding, contributes slightly favorably. Compared with 11j and 11k, ΔG_{ele} and ΔG_{vdw} of 11j (−28.31 and −57.35 kcal/mol) are stronger than those of 11k (−21.78 and −48.82 kcal/mol). However, as the penalty of ΔG_{PB}, the difference of the net electrostatic contributions between 11j and 11k is decreased from −6.53 to −1.91 kcal/mol. Therefore, ΔE_{vdw} plays the most important role in differentiating the activity between 11j and 11k.

Decomposition of the binding free energy

In order to gain a detailed picture of the inhibitor/p38α interactions, the binding free energy was decomposed into inhibitor-residue pairs. The quantitative information is extremely useful to understand the difference of the binding mechanism between 11j and 11k. The interactions between the inhibitors and the important residues of p38α are shown in Fig. 6.

From Fig. 6 one can see that both of the inhibitors share similar interaction mechanisms, which have stronger interactions with VAL38, ALA51, LYS53, GLU71, ILE84, LEU108 and LEU167 of p38α. And it is noteworthy to mention that MET109 plays distinct roles with 11j (−2.24 kcal/mol) and 11k (−0.11 kcal/mol). The interaction model of 11j is shown in Fig. 7. The phenyl group in Me-benzyl is close to LEU108 and the pyrrolo[2,1-f][1,2,4]triazine ring is located between VAL38 and LEU167. Comparison between 11j and 11k shows the interactions of 11j with ILE84, LEU108, MET109 and LEU167 (−1.68, −3.17, −2.24 and −3.82 kcal/mol) are stronger than those of 11k (−1.52, −1.13, 0.11 and −2.89 kcal/mol). However, the interaction between 11j and VAL38 (−1.45 kcal/mol) is weaker than that between 11k and VAL38 (−2.11 kcal/mol). Meanwhile it is interesting to observe that most of the residues belong to non-polar hydrophobic residues. So we infer that there should have

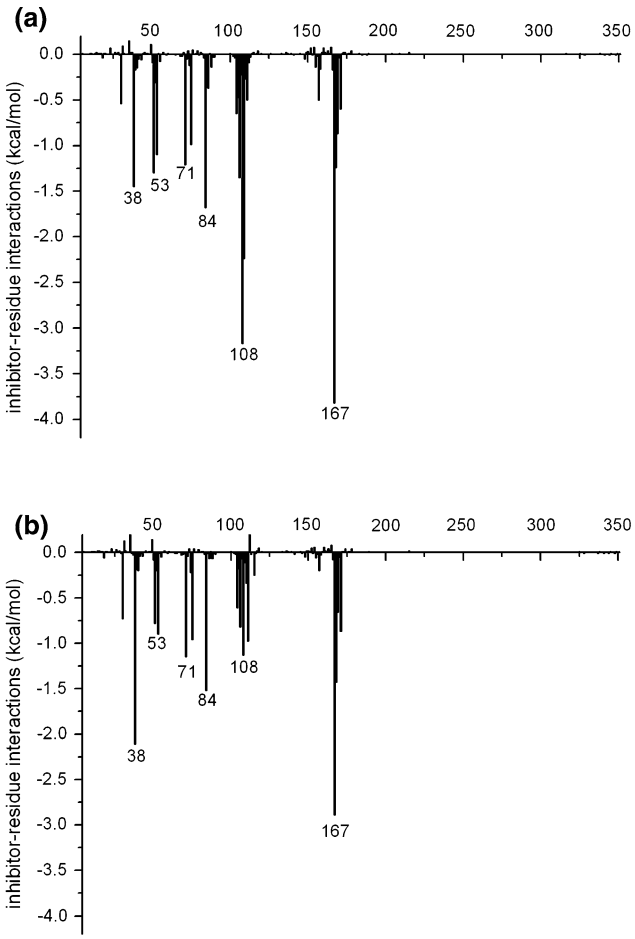

Fig. 6 Inhibitor–residue interaction spectrums of (**a**) the p38α/11j complex (**b**) the p38α/11k complex according to the MM/GBSA decomposition analysis. The *x*-axis represents the residue number of p38α

distinct difference of the van der Waals interaction between 11j and 11k with these residues, which leads to the large difference of the biological activities between 11j and 11k. In order to prove our inference, we compared the van der Waals interactions between inhibitors and the important residues. The results are shown in Fig. 8. As we expected distinct difference of the van der Waals interactions between 11j and 11k can be found, especially on three residues, i.e., VAL38, LEU108 and LEU167. The interactions of 11j with LEU108 and LEU167 (−2.20 and −2.52 kcal/mol) are stronger than those of 11k (−1.02 and −1.98 kcal/mol). However, the interaction of 11j with VAL38 (−1.24 kcal/mol) is weaker than that of 11k (−1.94 kcal/mol). The result

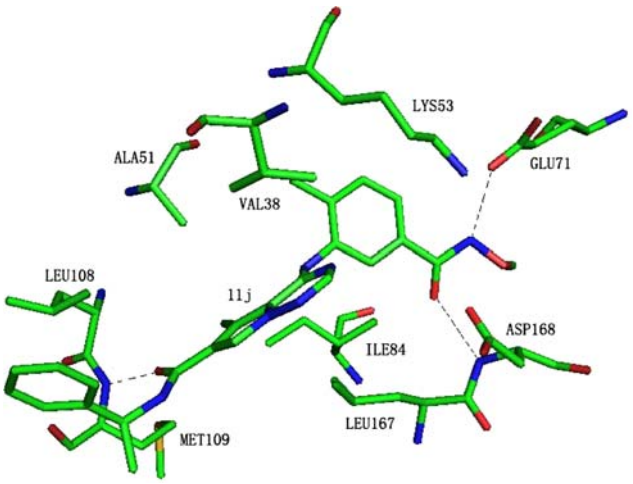

Fig. 7 Geometries of the residues that are essential to the binding free energies and model of hydrogen bonds between inhibitor and p38α

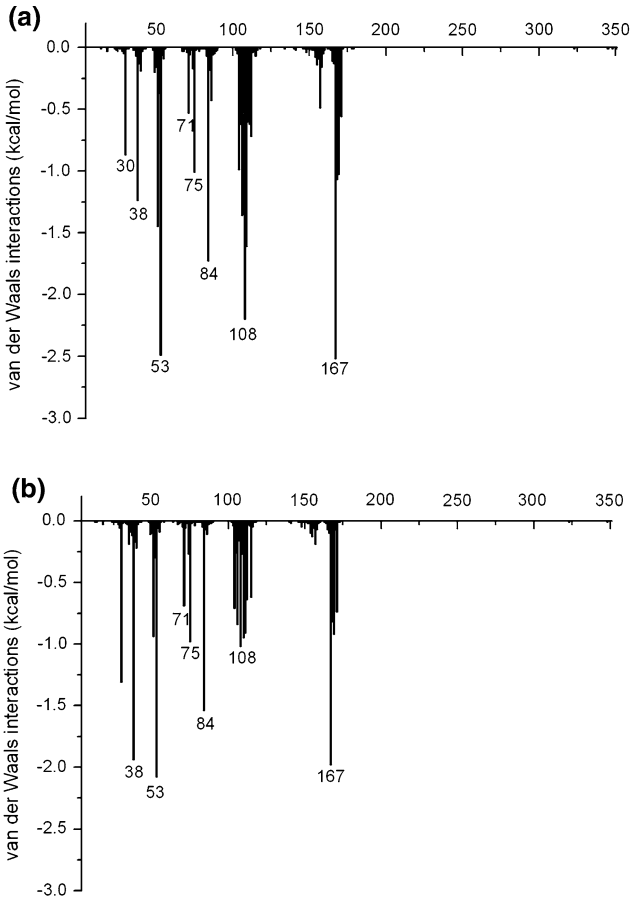

Fig. 8 The van der waals interaction spectrums between the inhibitors and the important residues of (**a**) the p38α/11j complex and (**b**) the p38α/11k complex

is consistent with the inhibitor–residue interaction in Fig. 6. Especially it is necessary to mention that the van der Waals interaction spectrums are quite similar to the inhibitor–residue interaction spectrums. Thus, it further supports our inference that the difference of the van der Waals interactions between ligand and protein determine the difference of the activities between 11j and 11k.

Then we wonder what role the electrostatic interaction plays in the binding of inhibitors with p38α, because it is reported that three hydrogen bonds form between each inhibitor and p38α [26]. The first forms between GLU71 and alkoxyamide NH, and the second between the backbone NH of ASP168 and the alkoxyamide carbonyl. Furthermore a hydrogen bond between the NH of MET109 and carbonyl of the C6 substituent which exists in most p38α inhibitors is also formed. The detailed interactions are shown in Fig. 7. Then we want to know what effect they play in the binding. For the purpose we analyzed ΔE_{ele} and compared it with ΔG_{PB}. The results are shown in Figs. 9 and 10.

From Fig. 9 it is clear that these two inhibitors have strong interactions with GLU71. The interaction of 11j (−7.08 kcal/mol) is stronger than that of 11k (−6.37 kcal/mol). Meanwhile the interaction of 11j with MET109 (−3.09 kcal/mol) is distinctly different from that of 11k (−0.46 kcal/mol). Two of the interactions are related to the hydrogen bonds we mentioned above. Then it is expect that the strong interaction between inhibitors and ASP168 can be found in Fig. 9, but unexpectedly the unfavorable interaction is found. In order to investigate the influence of the configuration on the hydrogen bond interaction, we computed the hydrogen bonds visible percentage during MD simulations. The result is shown in Table 2. We find that the percentage of the hydrogen bonds between MET109 and carbonyl on C6 substituent of 11k is distinctly smaller than that of 11j (76.90). The visible percentage of hydrogen bond is consistent with the analysis of the electrostatic interaction that the electrostatic interaction between 11j with MET109 is stronger than that between 11k and MET109.

In order to estimate the influence of the polar solvation free energy we analyzed the ΔG_{polar} term, and the result is shown in Fig. 10. The interaction is almost opposite to the electrostatic interaction, namely interaction with GLU71 and MET109 oppose the binding but the interaction with Asp168 is in favor of binding. On the whole, the net electrostatic interaction ($\Delta E_{ele} + \Delta G_{PB}$) opposes the binding. The result is consistent with the discussions in section "Binding free energy".

Analysis of the structures of the p38α/inhibitor complexes

All above analyses of the binding free energy have explained the reason why 11j is more active than 11k from the view of energy. In fact the energy is decided by the

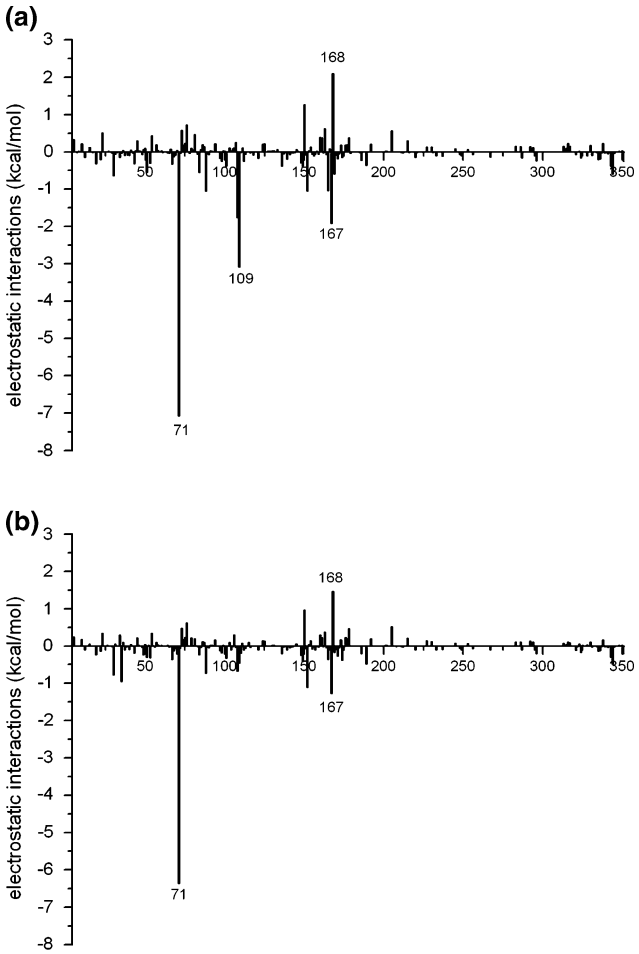

Fig. 9 The electrostatic interaction spectrums between the inhibitors and the important residues of (**a**) the p38α/11j complex and (**b**) the p38α/11k complex

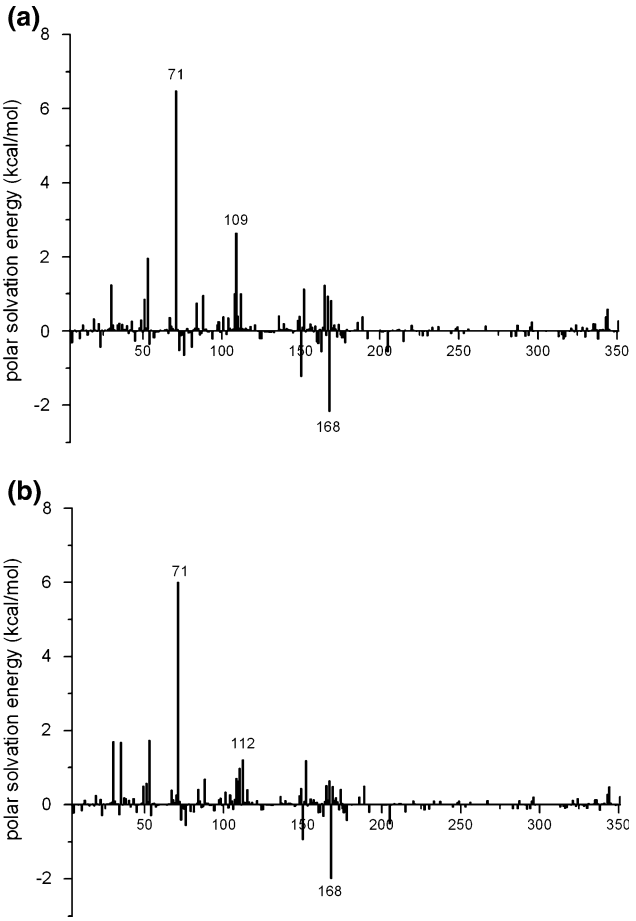

Fig. 10 The polar solvation free energy spectrums between the inhibitors and the important residues of (**a**) the p38α/11j complex and (**b**) the p38α/11k complex

structure. So we expect to know the detailed information how the R-configured group influences the binding and eventually changes the interaction with p38α. Here we analyzed the structures which may answer the question.

Firstly, we compared a series of p38α/11j snapshots from initial to the last dynamic structure. As it is impossible to list all snapshots during the dynamic simulation, we selected the initial complexed structure, the optimized structure and the snapshot at 4 ns to complain the phenomenon (Fig. 11a). As shown in Fig. 11a, the ligand 11j only undergoes little movement, that is to say, 11j is stable throughout the simulations.

Then we compared several p38α/11k snapshots from initial to the last dynamic structure as p38α/11j complex (see Fig. 11b). Compared with 11j, it is obvious that the (R)-α-Me-benzyl group of 11k has undergone a large movement after optimization, about 3.32 Å away from the initial position. After 4 ns MD simulations, the distance has increased to 5.00 Å. Influenced by the (R)-α-Me-benzyl group the pyrrolo[2,1-f][1,2,4]triazine group moves far away from LEU167, and then the interaction with LEU167 is decreased. However, the distance between the pyrrolo[2,1-f][1,2,4]triazine cycle and VAL38 is decreased after MD simulations. The structure explains the phenomenon why the interactions of 11j with LEU108 and LEU167 are stronger than those of 11k, but the interaction of 11j with VAL38 is weaker than that of 11k.

Conclusion

Inhibitors 11j and 11k with different configurations of the α-Me-benzyl group show distinct difference on the activity with p38α. In this work we analyzed the mechanism how different configurations influence the binding affinity using the molecular dynamics simulations, MM/PBSA free energy calculations and MM/GBSA free energy decomposition analysis. We find that the van der Waals interaction decide the activities and plays the most important role in differentiating the activities between 11j and 11k with p38α. The difference of the van der Waals interaction is

Table 2 Hydrogen bonds visible percentage during MD simulations

Inhibitor	Acceptor	Donor	Percentage (%)	Distance (Å)	Angle (°)
11j	:inhi@O2	:109@H-:109@N	76.90	2.86	17.16
	:inhi@O3	:168@H-:168@N	73.17	2.86	16.13
	:71@OE2	:inhi@H15-:inhi@N5	87.13	2.81	27.89
11k	:inhi@O2	:109@H-:109@N	0.00	4.46	36.08
	:inhi@O3	:168@H-:168@N	66.13	2.86	29.76
	:71@OE2	:inhi@H15-:inhi@N5	79.00	2.82	29.85

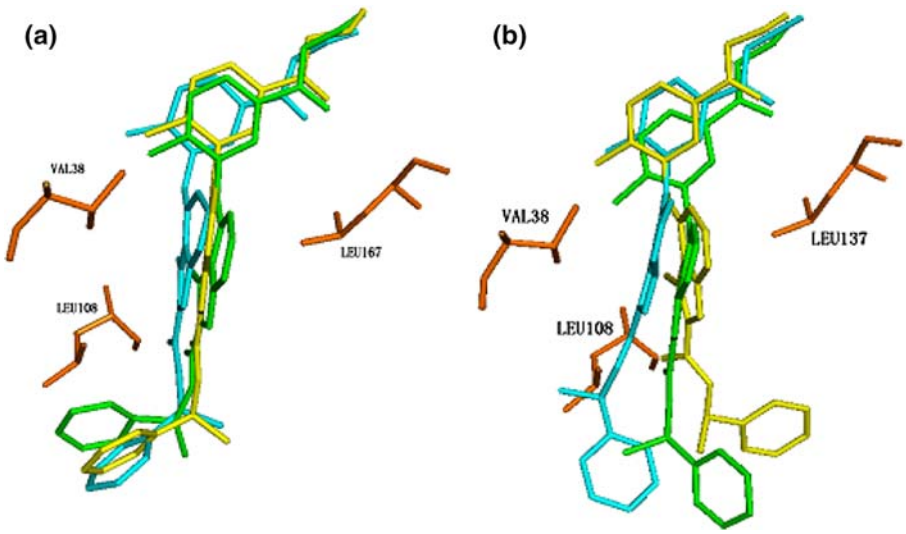

Fig. 11 Structure comparison of initial, optimized and the snapshot at 4 ns of (**a**) the p38α/11j complexes and (**b**) the p38α/11k complexes. The *yellow* one is the initial structure, the *green* one is minimized structure and the *cyan* one is the 4 ns snapshot

mainly determined by two residues, LEU108 and LEU167. Consequently stabilization of pyrrolo[2,1-f][1,2,4]triazine ring is important for the activities of inhibitors. Contrarily, the electrostatic interaction has little effect on the binding free energy because the strong electrostatic interaction between ligand and protein is effective compensated by the polar solvation free energy.

According to the energy decomposition and structure analysis, it can be found that the difference of the binding free energies between 11k and 11j were caused by the different configurations of the α-Me-benzyl group. In conclusion, from the work, it is feasible to estimate the difference of inhibitors with different configurations by molecular dynamics simulations and provides useful information for drug design.

Acknowledgments The project was supported by the Natural Science Foundation of China (No. 20373089). We thank Prof. Xiaojie Xu in Department of Chemistry of Peking University for providing access to computer software such as AMBER.

References

1. English JM, Cobb MH (2002) Pharmacological inhibitors of MAPK pathways. Trends Pharmacol Sci 23:40–45
2. Salituro FG, Germann UA, Wilson KP, Bemis GW, Fox T, Su MSS (1999) Inhibitors of p38 MAP kinase: therapeutic intervention in cytokine-mediated diseases. Curr Med Chem 6:807–823
3. Foster ML, Halley F, Souness JE (2000) Potential of p38 inhibitors in the treatment of rheumatoid arthritis. Drug News & Perspect 13:488–497
4. Kumar S, Boehm J, Lee JC (2003) p38 map kinases: key signalling molecules as therapeutic targets for inflammatory diseases. Nat Rev Drug Discov 2:717–726
5. Saklatvala J (2004) The p38 MAP kinase pathway as a therapeutic target in inflammatory disease. Curr Opin Pharmacol 4:372–377
6. Choy EHS, Panayi GS (2001) Mechanisms of disease: cytokine pathways and joint inflammation in rheumatoid arthritis. N Engl J Med 344:907–916
7. Han J, Lee JD, Bibbs L, Ulevitch RJ (1994) A map kinase targeted by endotoxin and hyperosmolarity in mammalian-cells. Science 265:808–811
8. Han JH, Lee JD, Tobias PS, Ulevitch RJ (1993) Endotoxin induces rapid protein-tyrosine phosphorylation in 70z/3 cells expressing Cd14. J Biol Chem 268:25009–25014
9. Jiang Y, Chen CH, Li ZJ, Guo W, Gegner JA, Lin SC, Han JH (1996) Characterization of the structure and function of a new mitogen-activated protein kinase (p38 beta). J Biol Chem 271: 17920–17926
10. Lechner C, Zahalka MA, Giot JF, Moller NPH, Ullrich A (1996) ERK6, a mitogen-activated protein kinase involved in C2C12 myoblast differentiation. Proc Natl Acad Sci USA 93: 4355–4359

11. Li ZJ, Jiang Y, Ulevitch RJ, Han JH (1996) The primary structure of p38 gamma: a new member of p38 group of MAP kinases. Biochem Biophys Res Commun 228:334–340
12. Cuenda A, Dorow DS (1998) Differential activation of stress-activated protein kinase kinases SKK4/MKK7 and SKK1/MKK4 by the mixed-lineage kinase-2 and mitogen-activated protein kinase kinase (MKK) kinase-1. Biochem J 333:11–15
13. Kumar S, McDonnell PC, Gum RJ, Hand AT, Lee JC, Young PR (1997) Novel homologues of CSBP/p38 MAP kinase: activation, substrate specificity and sensitivity to inhibition by pyridinyl imidazoles. Biochem Biophys Res Commun 235:533–538
14. Jiang Y, Gram H, Zhao M, New LG, Gu J, Feng LL, DiPadova F, Ulevitch RJ, Han JH (1997) Characterization of the structure and function of the fourth member of p38 group mitogen-activated protein kinases, p38 delta. J Biol Chem 272:30122–30128
15. Fearns C, Kline L, Gram H, Di Padova F, Zurini M, Han J, Ulevitch RJ (2000) Coordinate activation of endogenous p38 alpha, beta, gamma, and delta by inflammatory stimuli. J Leukoc Biol 67:705–711
16. Allen M, Svensson L, Roach M, Hambor J, McNeish J, Gabel CA (2000) Deficiency of the stress kinase p38 alpha results in embryonic lethality: characterization of the kinase dependence of stress responses of enzyme-deficient embryonic stem cells. J Exp Med 191:859–869
17. Hale KK, Trollinger D, Rihanek M, Manthey CL (1999) Differential expression and activation of p38 mitogen-activated protein kinase alpha, beta, gamma, and delta in inflammatory cell lineages. J Immunol 162:4246–4252
18. Cirillo PF, Pargellis C, Regan JT (2002) The non-diaryl heterocycle classes of p38 MAP kinase inhibitors. Curr Top Med Chem 2:1021–1035
19. Kumar S, Blake SM (2005) Pharmacological potential of p38 MAPK inhibitors. In: Inhibitors of protein kinases and protein phosphates, vol 167. pp 65–83
20. Adams JL, Badger AM, Kumar S, Lee JC (2001) p38 MAP kinase: molecular target for the inhibition of pro-inflammatory cytokines. Prog Med Chem 38:1–60
21. Jackson PF, Bullington JL (2002) Pyridinylimidazole based p38 MAP kinase inhibitors. Curr Top Med Chem 2:1011–1020
22. Lee JC, Kumar S, Griswold DE, Underwood DC, Votta BJ, Adams JL (2000) Inhibition of p38 MAP kinase as a therapeutic strategy. Immunopharmacology 47:185–201
23. Leftheris K, Ahmed G, Chan R, Dyckman AJ, Hussain Z, Ho K, Hynes J, Letourneau J, Li W, Lin SQ et al (2004) The discovery of orally active triaminotriazine aniline amides as inhibitors of p38 MAP kinase. J Med Chem 47:6283–6291
24. Gill AL, Frederickson M, Cleasby A, Woodhead SJ, Carr MG, Woodhead AJ, Walker MT, Congreve MS, Devine LA, Tisi D (2005) Identification of novel p38 alpha MAP kinase inhibitors using fragment-based lead generation. J Med Chem 48:414–426
25. Goldberg DR, Hao MH, Qian KC, Swinamer AD, Gao DHA, Xiong Z, Sarko C, Berry A, Lord J, Magolda RL (2007) Discovery and optimization of p38 inhibitors via computer-assisted drug design. J Med Chem 50:4016–4026
26. Hynes J, Dyckman AJ, Lin SQ, Wrobleski ST, Wu H, Gillooly KM, Kanner SB, Lonial H, Loo D, McIntyre KW (2008) Design, synthesis, and anti-inflammatory properties of orally active 4-(phenylamino)-pyrrolo[2, 1-f][1, 2, 4]triazine p38 alpha mitogen-activated protein kinase inhibitors. J Med Chem 51:4–16
27. Huo SH, Wang JM, Cieplak P, Kollman PA, Kuntz ID (2002) Molecular dynamics and free energy analyses of cathepsin D-inhibitor interactions: insight into structure-based ligand design. J Med Chem 45:1412–1419
28. Kuhn B, Kollman PA (2000) Binding of a diverse set of ligands to avidin and streptavidin: an accurate quantitative prediction of their relative affinities by a combination of molecular mechanics and continuum solvent models. J Med Chem 43:3786–3791
29. Weis A, Katebzadeh K, Soderhjelm P, Nilsson I, Ryde U (2006) Ligand affinities predicted with the MM/PBSA method: dependence on the simulation method and the force field. J Med Chem 49:6596–6606
30. Wang JM, Morin P, Wang W, Kollman PA (2001) Use of MM-PBSA in reproducing the binding free energies to HIV-1 RT of TIBO derivatives and predicting the binding mode to HIV-1 RT of efavirenz by docking and MM-PBSA. J Am Chem Soc 123:5221–5230
31. Hou TJ, Chen K, McLaughlin WA, Lu BZ, Wang W (2006) Computational analysis and prediction of the binding motif and protein interacting partners of the Abl SH3 domain. Plos Comput Biol 2:46–55
32. Hou TJ, Guo SL, Xu XJ (2002) Predictions of binding of a diverse set of ligands to gelatinase-A by a combination of molecular dynamics and continuum solvent models. J Phys Chem B 106:5527–5535
33. Hou TJ, Yu R (2007) Molecular dynamics and free energy studies on the wild-type and double mutant HIV-1 protease complexed with amprenavir and two amprenavir-related inhibitors: mechanism for binding and drug resistance. J Med Chem 50:1177–1188
34. Wang JM, Hou TJ, Xu XJ (2006) Recent advances in free energy calculations with a combination of molecular mechanics and continuum models. Curr Comput-Aided Drug Des 2:287–306
35. Kollman PA, Massova I, Reyes C, Kuhn B, Huo SH, Chong L, Lee M, Lee T, Duan Y, Wang W (2000) Calculating structures and free energies of complex molecules: combining molecular mechanics and continuum models. Acc Chem Res 33:889–897
36. Hou TJ, McLaughlin W, Lu B, Chen K, Wang W (2006) Prediction of binding affinities between the human amphiphysin-1 SH3 domain and its peptide ligands using homology modeling, molecular dynamics and molecular field analysis. J Proteome Res 5:32–43
37. Hou TJ, Zhang W, Case DA, Wang W (2008) Characterization of domain-peptide interaction interface: a case study on the amphiphysin-1 SH3 domain. J Mol Biol 376:1201–1214
38. Gohlke H, Case DA (2004) Converging free energy estimates: MM-PB(GB)SA studies on the protein–protein complex Ras-Raf. J Comput Chem 25:238–250
39. Hou T, McLaughlin WA, Wang W (2008) Evaluating the potency of HIV-1 protease drugs to combat resistance. Proteins 71:1163–1174
40. SYBYL molecular simulation package (2004) http://www.sybyl.com
41. Case DA, Cheatham TE, Darden T, Gohlke H, Luo R, Merz KM, Onufriev A, Simmerling C, Wang B, Woods RJ (2005) The Amber biomolecular simulation programs. J Comput Chem 26:1668–1688
42. Duan Y, Wu C, Chowdhury S, Lee MC, Xiong GM, Zhang W, Yang R, Cieplak P, Luo R, Lee T (2003) A point-charge force field for molecular mechanics simulations of proteins based on condensed-phase quantum mechanical calculations. J Comput Chem 24:1999–2012
43. Frisch MJ, Trucks GW, Schlegel HB, Scuseria GE, Robb MA, Cheeseman JR, Montgomery JAJ, Vreven T, Kudin KN, Burant JC et al (2004) Gaussian 03. Gaussian Inc., Wallingford CT
44. Bayly CI, Cieplak P, Cornell WD, Kollman PA (1993) A well-behaved electrostatic potential based method using charge restraints for deriving atomic charges—the resp model. J Phys Chem 97:10269–10280
45. Wang JM, Wolf RM, Caldwell JW, Kollman PA, Case DA (2004) Development and testing of a general amber force field. J Comput Chem 25:1157–1174

46. Jorgensen WL, Chandrasekhar J, Madura JD, Impey RW, Kleins ML (1983) Comparison of simple potential functions for simulating liquid water. J Chem Phys 79:926–935
47. Berendsen HJC, Postma JPM, Vangunsteren WF, Dinola A, Haak JR (1984) Molecular-dynamics with coupling to an external bath. J Chem Phys 81:3684–3690
48. Ryckaert JP, Ciccotti G, Berendsen HJC (1977) Numerical-integration of cartesian equations of motion of a system with constraints—molecular-dynamics of *N*-alkanes. J Comput Phys 23: 327–341
49. Darden T, York D, Pedersen L (1993) Particle Mesh Ewald: an N·Log(N) method for Ewald sums in large systems. J Chem Phys 98(12):10089
50. Weiser J, Shenkin PS, Still WC (1999) Approximate atomic surfaces from linear combinations of pairwise overlaps (LCPO). J Comput Chem 20:217–230
51. Onufriev A, Bashford D, Case DA (2004) Exploring protein native states and large-scale conformational changes with a modified generalized born model. Proteins 55:383–394